Deep-Sea Research, Vol. 31, No. 5, pp. 551–569, 1984.
Printed in Great Britain.

0198-0149/84 $3.00 + 0.00

Objective analysis of simulated equatorial Atlantic Ocean data on seasonal time scales

M. J. McPHADEN,* G. REVERDIN,† J. MERLE,‡ Y. DU PENHOAT‡ and A. KARTAVTSEFF†

(*Received* 23 *August* 1983; *in revised form* 28 *December* 1983; *accepted* 5 *March* 1984)

Abstract—In this study we objectively analyze simulated equatorial Atlantic Ocean data on seasonal time scales using a technique based on optimal interpolation. The purpose is twofold: (1) to estimate the accuracy of the FOCAL/SEQUAL (Programme Francais Ocean-Climat en Atlantique Equatorial/Seasonal Equatorial Atlantic Response Program) array for mapping large-scale seasonal variations in the depth of the 20° isotherm, and (2) to examine the potential of 20 FOCAL drifting buoys drogued with thermistor chains for enhancing that mapping accuracy. This latter point leads to the development of a heuristic model for drifter motion in order to identify the most favorable time and location for buoy deployments. Results are discussed for a number of assumptions about oceanic variability required by both the optimal interpolation procedure and the drifting buoy model. From these we conclude that with data provided by the FOCAL/SEQUAL array, excluding FOCAL drifters, one can expect to map large-scale seasonal variations in the depth of the 20°C isotherm to within 5 m over about 65% of the equatorial Atlantic. This region of expected 5 m accuracy expands to nearly 90% of the equatorial Atlantic if FOCAL drifters are deployed between 2 and 4°S at 5°W in four quarterly installments of five each. Drifters deployed further to the east or to the west will be less useful in defining large-scale, low-frequency thermal variations since they do not disperse as widely as do those deployed at 5°W.

1. INTRODUCTION

SEASONAL variations in both the current and temperature fields are very pronounced in the equatorial Atlantic as inferred from historical data. The North Equatorial Countercurrent (NECC) is present as a continuous band of zonal flow west of 20°W only during northern summer and fall. Likewise, both the South Equatorial Current (SEC) along the equator and the Guinea Current in the Gulf of Guinea are at their strongest in the latter part of the year. Equatorial Undercurrent (EUC) transports, though less well documented than surface flows, exhibit a tendency for large values in late winter and smaller values in spring and summer (KATZ *et al.*, 1981). Sea surface temperature (SST) displays a marked seasonality with the development in summer of an intense cold tongue along the equator and a marked cooling in the Gulf of Guinea. Dynamic topography of the sea surface, oceanic heat content relative to 300 m, and the depth of the 20°C isotherm likewise exhibit large seasonal fluctuations (MERLE, 1983). From March to August in all three a very sharp ridge/trough system develops in the meridional direction to geostrophically balance the NECC and enhanced SEC, and the zonal slope along the equator increases by a factor of ~2 (e.g., Fig. 1 and KATZ *et al.*, 1977).

* The Joint Institute for the Study of the Atmosphere and Ocean, University of Washington, Seattle, WA 98195, U.S.A.

† Laboratoire d'Oceanographie Physique, Museum National d'Histoire Naturelle, 43–45 rue Cuvier, 75231 Paris cedex 05, France.

‡ Antenne ORSTOM, Centre Oceanologique de Bretagne, B.P. 337 29273, cedex, France.

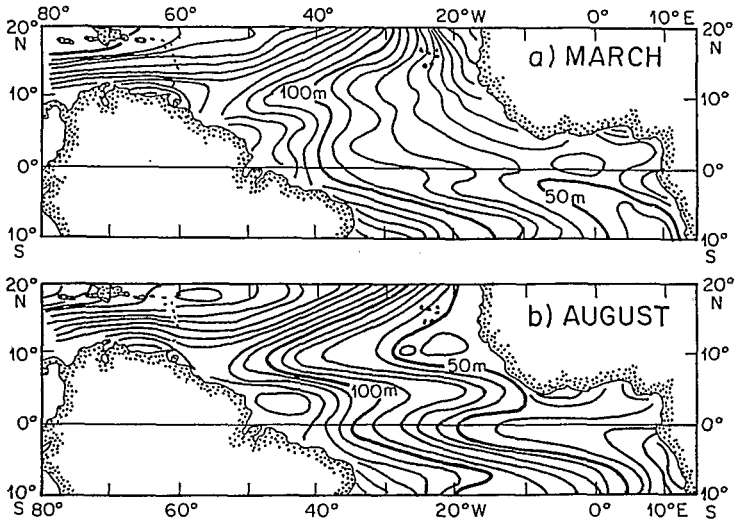

Fig. 1. Climatological mean depth of the 20°C isotherm for months of (a) March and (b) August, based on historical hydrographic data. Contour interval is 10 m.

Similar variations are observed in the depth of the thermocline, defined as the depth of maximum vertical temperature gradient (ROBERT HOUGHTON, Lamont-Doherty Geological Observatory, personal communication).

Associated with these oceanic fluctuations are equally pronounced changes in surface winds. During northern winter, the Northeast (NE) Trades are strong, the Southeast (SE) Trades relatively weak, and the Intertropical Convergence Zone (ITCZ) is close to the equator. During northern summer the NE Trades weaken, the SE Trades intensify, and the ITCZ migrates northward to about 10°N. A number of theories have been proposed to explain the dynamical connections between such wind variations and the ocean's response (MOORE *et al.*, 1978; PHILANDER, 1979; PHILANDER and PACANOWSKI, 1981; CANE and SARACHIK, 1981; MCCREARY *et al.*, 1984) and from these we have gained valuable insights into the physics of wind-driven seasonal variability in the equatorial Atlantic. However, a deeper understanding of relevant physical processes has been hampered by the lack of comprehensive, synoptic, oceanic and atmospheric data sets against which dynamical hypotheses can be tested more critically.

FOCAL (Programme Francais Ocean-Climat en Atlantique Equatorial) and SEQUAL (Seasonal Equatorial Atlantic Response Program) are collaborative observational and modeling programs which share a common goal: understanding the dynamics of seasonal variability in the equatorial Atlantic. By closely coordinating their efforts FOCAL, sponsored by the French government, and SEQUAL, funded primarily by the National Science Foundation, will continuously monitor several oceanic and atmospheric variables over two complete realizations of the seasonal cycle beginning in mid-1982. The bulk of the FOCAL/SEQUAL field array is shown in Fig. 2. It is composed of a diversity of elements concentrated between 10°E and 50°W, 6°S and 10°N, most of which are in place specifically for the 2-year intensive sampling period, although the XBT lines and tide gauge stations could be viewed as components of a longer term array as well. All instrument systems will sample with regularity throughout several seasons, with the exception of the AXBTs, which will be used for burst

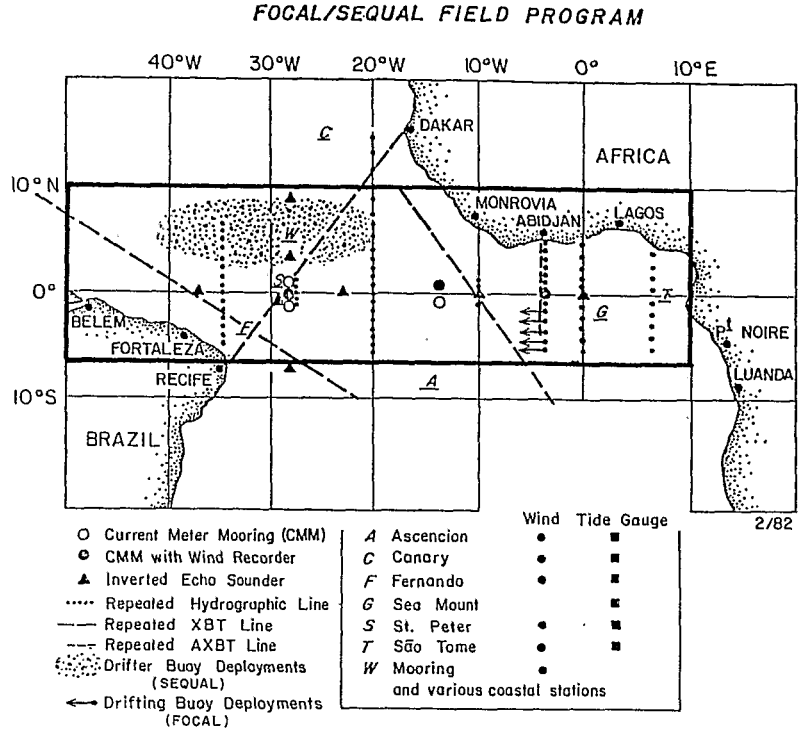

Fig. 2. Components of the FOCAL/SEQUAL field array. Current meter moorings will also measure temperature at several depths and thermistor chains will be attached to the FOCAL drifting buoys. SEQUAL drifters deployed in the NECC region will not be drogued by thermistor chains and therefore will not monitor the subsurface temperature fields. The region 10°E to 50°W, 6°S to 10°N is outlined in heavy black (after ANON., 1982).

sampling during the summer upwelling season in the Gulf of Guinea. Of special interest in this study are the FOCAL drifters. A total of 20 will be deployed in four installments of five each beginning in June 1983. In contrast to the SEQUAL drifters, which have a window shade drogue at 30 m, these will be equipped with 115 m long thermistor chains plus window shade drogues at 15 m. Satellites will track them by the ARGOS system (BESSIS, 1982) and relay data back to ground stations about 4 to 6 times a day. The location of their deployment indicated in Fig. 2 is a result of this study, one which will be elaborated on shortly.

The FOCAL/SEQUAL array will return a large quantity of high quality data which can be used to test dynamical hypotheses concerning the equatorial ocean response to seasonal wind forcing. The temperature field will be especially well sampled, since almost all platforms will measure either directly or by proxy some quantity related to the thermal structure. A convenient and sensible way to summarize this information is to draw maps which can be used for descriptive purposes, for diagnostic studies, and for initialization and verification of ocean models. The purpose of this study is therefore to explore a univariate objective analysis technique for mapping temperature data from the field array using the depth of the 20°C isotherm as an example. This parameter is of obvious dynamical relevance because over large portions of the equatorial Atlantic it is well correlated with the thermocline depth, dynamic height, and integrated heat content. It is likewise convenient to work with because its

climatology is well defined (Fig. 1). Moreover, the FOCAL/SEQUAL experiment will provide more new information on the depth of the 20°C isotherm than on either dynamic height or integrated heat content, because computation of the former requires salinity data which will be available only from CTD measurements, and computation of the latter, to be a useful indicator of ocean dynamics vis-à-vis surface thermodynamics, requires temperature measurements at depths of a few hundred meters. Of course one could and should analyze these other fields as well, since though well correlated with the depth of the 20°C isotherm, there are some significant differences. Nonetheless, we will restrict ourselves in this study to the analysis of the 20°C isotherm with the caveat that alone it does not contain all the useful information on internal thermal variability.

The particular questions that we will address are (1) how accurately can we expect to map seasonal variations in the depth of the 20°C isotherm from the FOCAL/SEQUAL array; and (2) are drifting buoys an effective means of monitoring these variations, and if so, how are they best deployed for that purpose? The first question is motivated by the fact that the value of mapped data for any of the uses noted above is directly proportional to the accuracy of such maps. It is therefore desirable to have some estimate of how the FOCAL/SEQUAL array might perform in this regard. The second question arises because the FOCAL drifters will function both as temperature sensors and current meters. The rationale that guides their deployment will differ depending on which mode of operation is emphasized. In this study we focus on the drifters as temperature sensors and illustrate their utility in that mode.

The technique used in this paper is based on optimal interpolation and is fully described in BRETHERTON *et al.* (1984; hereafter referred to as BMK). There it was used to design an XBT network for detecting changes in heat content in the North Atlantic on climatological time scales. In this study, as in BMK, conclusions will be based on simulated data although ultimately it is the analysis of real data we are interested in.

The remainder of this paper is organized as follows. Section 2 summarizes the BMK methodology and its adaptation to the FOCAL/SEQUAL design study. In Section 3 we develop a heuristic model of drifting buoy motion and examine the simulated trajectories of several different deployments. Based on these simulations we suggest that the most favorable location for FOCAL drifter deployments is approximately 5°W, 2 to 4°S. We then show expected errors in maps of the 20°C isotherm depth derived from a number of different arrays, including a long-term array of XBTs and tide gauges and the FOCAL/SEQUAL array with and without FOCAL drifters. For simplicity, AXBTs are not included in these arrays because they will be deployed during only a few summer weeks and are relatively few in number. SEQUAL drifters are likewise not included because they will not be drogued with thermistor chains (although in a multivariate objective analysis drifter velocity could be used to infer subsurface temperature variations as well). Our basic conclusions, summarized in Section 4, are that on seasonal time-scales the FOCAL/SEQUAL array can achieve 5 m accuracy over large areas of the equatorial domain, and that FOCAL drifters contribute significantly to this accuracy if deployed at 5°W between 2 and 4°S.

2. METHODOLOGY

Objective analysis can be loosely defined as any mathematical procedure for transforming irregularly spaced observations into a field of smoothed estimates at regularly spaced grid points. A number of well-known techniques satisfy this definition, including regression analysis (DRAPER and SMITH, 1966), successive corrections methods (CRESSMAN, 1959), and

optimal interpolation (GANDIN, 1965). This latter technique requires reasonably accurate *a priori* information regarding the statistics of signal and noise variability in the region of interest. Given this information, estimates are optimal in the sense that no more accurate linear combinations of the observations exist based on a least squares criterion. Optimal interpolation also has the advantage that in addition to yielding smoothed estimates of a particular variable, it yields an expected error in these estimates. This feature has been exploited in previous oceanographic array design studies (BMK; BRETHERTON *et al.*, 1976), in which different array configurations are used to analyze computer simulated data generated from the assumed signal and noise statistics. One array is then selected as the most cost-effective based on a consideration of overall accuracy for a given level of effort and fixed number of resources. In this study we begin with an array which, with the exception of the FOCAL drifters, has been already set. The design of this array was based on the collective experience of the individual FOCAL and SEQUAL principle investigators rather than computer-based techniques and it is intended to investigate a diversity of phenomena on different time and space scales. We will examine one aspect of this array design, namely its accuracy for mapping large-scale seasonal variations in the depth of the 20°C isotherm and, in addition, the contribution that FOCAL drifters can make to that accuracy. The methodology employed in this paper is that of BMK, a variant of GANDIN's (1965) linear estimation theory, in which signal statistics are specified in frequency-wavenumber space rather than in physical space. A brief summary of the BMK theory for optimal interpolation of a single scalar variable (in our case the 20°C isotherm depth) is presented below.

Define an observation of the 20°C isotherm depth as

$$h(\mathbf{x}, t) = h_0(\mathbf{x}, t) + h'(\mathbf{x}, t) + \varepsilon(\mathbf{x}, t), \tag{1}$$

where h_0 is a seasonal climatology based on historical data analyses like that shown in Fig. 1, h' is a large-scale seasonal anomaly about this climatology which we will term signal, and ε is observational noise due to the combined effect of unresolved high-frequency geophysical processes and instrumental noise. We will assume for the moment that the climatology h_0 is known exactly. Signal, sometimes referred to as prediction error in the meteorological literature (LORENC, 1981), then consists of interannual deviations occurring naturally in a particular region. It is distinguished from noise by scale; i.e. it is defined to be those scales in frequency-wavenumber space that are adequately resolved by a sparse, large-scale array and for which reasonable estimates can be made. Geophysical noise, on the other hand, consists of such mesoscale phenomena as high-frequency equatorial waves and mean current meanders, as well as local meteorologically induced thermal variations, internal tides, etc., whose spatial structures are not well-resolved and whose effects, together with instrumental noise, we want to filter out by the interpolation procedure.

Optimal interpolation requires that these statements about signal and noise be formulated into mathematical expressions in order to analyze a particular set of observations. Thus, we represent the signal in terms of a truncated Fourier series

$$h'(\mathbf{x}, t) = \sum_{m=1}^{M} \lambda_m f_m(\mathbf{x}, t), \tag{2}$$

where λ_m, $m = 1, \ldots M$ are spectral coefficients assumed to be joint normally distributed with zero mean and covariance given by the matrix expression

$$P^{-1}_{mn} = \langle \lambda_n \lambda_m \rangle. \tag{3}$$

Angle brackets denote ensemble average, or by the ergodic theorem (which we assume holds), time average. The spectral functions f_m are given by

$$\{f_m\} = a_m \begin{cases} \begin{bmatrix} 1 \\ x - \frac{1}{2} \\ y - \frac{1}{2} \end{bmatrix} \times \begin{bmatrix} \cos(2\pi\omega t) \\ \sin(2\pi\omega t) \end{bmatrix} & \text{(4a)} \\ \begin{bmatrix} \cos(2\pi kx) \\ \sin(2\pi kx) \end{bmatrix} \times \begin{bmatrix} \cos(2\pi ly) \\ \sin(2\pi ly) \end{bmatrix} \times \begin{bmatrix} \cos(2\pi\omega t) \\ \sin(2\pi\omega t) \end{bmatrix} & \text{(4b)} \end{cases}$$

$$1 \leqslant k + l \leqslant 3$$

$$0 \leqslant \omega \leqslant 2,$$

where x is the zonal coordinate scaled by 60° of longitude, y is the meridional coordinate scaled by 16° latitude, and t is time scaled by 1 year. The notation in (4) implies that each element of the set f_m is a unique product of elements in the bracketed subsets with no subset represented by more than one element at a time. The constants a_m are chosen such that the time/space averaged variance of each f_m is equal to 1. Spatial means and trends are included in (4a) whereas harmonic spatial variations are included in (4b). In the latter we have allowed up to 3 wavelengths per basin dimension in each direction, i.e., wavelengths as short as 2000 km zonally and 500 km meridionally. This particular truncation mimics the observed anisotropy on a horizontal plane and includes those wavenumbers expected to be most energetic on seasonal time scales. Frequencies up to 2 cycles per year (cpy) have been included though it is assumed for simplicity that there are no time trends over the course of a year. In all, there are 135 spectral functions represented in (4) if the frequency cutoff is $\omega = 2$, and 81 if the cutoff is $\omega = 1$.

Stationarity and, at least initially, homogeneity are assumed. Together, these imply that spectral components are uncorrelated, so that P_{mn} reduces to a diagonal matrix with each element equal to the expected variance in a particular frequency-wavenumber band. We prescribe the total variance integrated across all frequencies and wavenumbers such that it is equivalent to a 15 m root-mean-square (r.m.s.) deviation from climatology consistent with Merle's ongoing analysis of the historical record. This is divided equally into time mean and time varying components with spectral energy in the latter distributed according to a -2 power law in frequency. Within each frequency band, moreover, we have assigned the signal a -2 scalar wavenumber slope like that found in the tropical Pacific for low-frequency, large-scale, thermal variations (WHITE *et al.*, 1982). Specifically, this implies $\int P(k, l)\mathrm{d}l \propto k^{-2}$ and $\int P(k, l)\mathrm{d}k \propto l^{-2}$ (where for discrete spectra the integral is replaced by a summation over wavenumber bands). Specification of the signal is completed by prescribing the total energy in these spatial variations to be 1.5 times that of spatial average and trends.

One can multiply each spectral coefficient by a Gaussian random number to construct different realizations of these signal statistics. In two such realizations (Fig. 3), zonal scales of about 10° longitude and meridional scales of about 2° latitude are evident, as are 0 (15 m) magnitudes. Our assertion is that anomalies such as this are likely on seasonal time scales in the tropical Atlantic. Also shown in Fig. 3 is our approximation of the oceanic domain on 2° × 2° resolution. Such coarse definition of the boundaries, together with the above definition of signal, essentially exclude coastal regions from the type of large-scale analysis that we are considering.

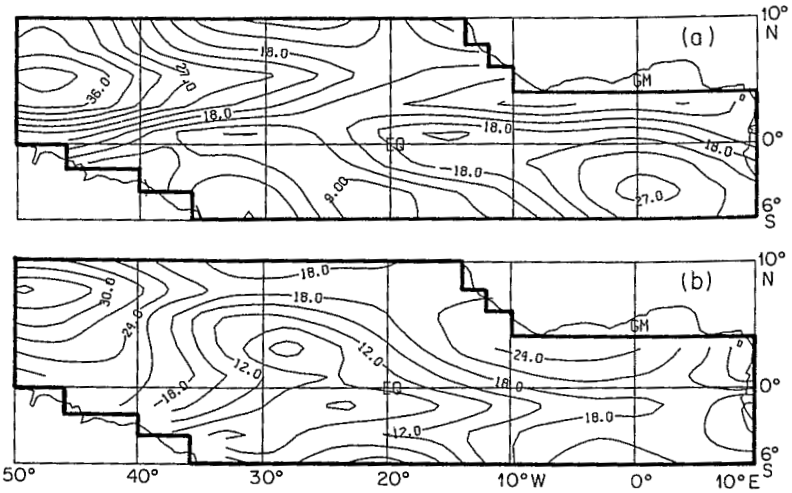

Fig. 3. Two realizations of the 20°C isotherm depth anomaly on seasonal time scales generated from the signal statistics discussed in Section 2. Contours are r.m.s. deviation from climatology, i.e., $(h'^2)^{\frac{1}{2}}$, derived from 1 year of data. Contour interval is 3 m. Grid is 2° latitude by 2° longitude in this and subsequent contoured maps. Definition of oceanic boundaries is shown in heavy black.

We note that there is nothing special about the use of sines and cosines as our spectral functions in (2). Any set of functions, for example, Hermite or Legendre functions, would do as long as they are complete with respect to the assumed scales of signal variance. Our choice of trigonometric functions in this regard is strictly a matter of programming convenience.

Noise is due to both instrumental errors and aliased geophysical variability. With respect to instrumental noise, we assume that an intercalibration has been done to remove systematic differences between platforms and that otherwise all platforms are equally accurate except for the tide gauges and inverted echo sounders (IES). These latter two platforms do not measure temperature directly, but rather sea level and integrated sound speed, respectively. Both types of measurement are significantly, although imperfectly, correlated with the 20°C isotherm depth or some related quantity such as dynamic height (WYRTKI, 1974; MILLER, 1981). Taking this correlation coefficient to be 0.7 establishes the weight given to tide gauges and IES relative to other array elements (Table 1).

We have weighted XBT, CTD mooring, and drifting thermistor chain data identically even though we know, for example, that XBTs may be less accurate than CTDs by ±5 m in the upper few hundred meters of the ocean (SEAVER and KULESHOV, 1982). This is because random instrumental noise in all cases is much weaker than that due to aliased energetic oceanic fluctuations which appear as white noise in the resolved portion of the spectrum. It is this geophysical noise which is of greatest concern in determining the accuracy of the FOCAL/SEQUAL array. We will assume that this noise manifests itself as a Gaussian random process which has zero mean and covariance between observations at $(\mathbf{x}, t)_i$ and $(\mathbf{x}, t)_j$ of

$$\langle \varepsilon_i \varepsilon_j \rangle = \sigma_{ij}^2 \tag{5}$$

but which is uncorrelated with the signal, i.e.,

$$\langle \varepsilon \lambda \rangle = 0. \tag{6}$$

Table 1. *Nominal sample rates in time* (Δt) *and, for moving platforms, in distance* (Δd), *as well as the relative weight assigned to data from each platform*

Platform	Sample rate	Weight
1. XBT	$\Delta t = 60$ days $\Delta d = 175$ km along each track	1.0
2. CTD	$\Delta t = 90$ days $\Delta d = 100$ km along each track	1.0
3. Moorings	$\Delta t = 10$ days	1.0
4. Inverted echo sounders (IES)	$\Delta t = 10$ days	0.7
5. Tide gauges	$\Delta t = 10$ days	0.7
6. FOCAL drifters	$\Delta t = 10$ days $\Delta d =$ variable	1.0

Stationarity and, for the moment, homogeneity are assumed with a magnitude equivalent to a 15 m s.d. from the mean. Decorrelation time space scales inferred from a number of studies (DÜING *et al.*, 1975; WEISBERG, 1979) are set at 10 days, 2° longitude, and 1/2° latitude. These scales determine the minimum spacing between independent estimates of the seasonal signal and are incorporated into the analysis scheme by discarding all those observations separated by smaller distances in space and time. Hence sample rates in Table 1 for tide gauges, IES, moorings, and drifting thermistor chains reflect these decorrelation time scales rather than actual sample rates, which in some cases are on the order of minutes. We note that when dealing with real data it may be more advantageous to average neighboring observations into a 'superobservation' rather than winnow them. This produces a slightly more accurate datum due to the reduction of any instrumental noise and/or short-term oceanic fluctuations of small amplitude. Thus, for example, one would weight a 10-day average of mooring data higher than a single CTD cast because tides and small-scale internal waves have been averaged out of the former. Accounting for this in the present study would not alter our basic conclusions however, because as at mid-latitudes it is the mesoscale which is the dominant source of aliased variability in large, climate-scale arrays.

The above definitions of signal and noise we will refer to collectively as our standard assembly. This assembly is idealized and cannot be rigorously defended as accurate in every detail. As such it should be considered an initial hypothesis and a benchmark for sensitivity tests in which alternate assemblies are examined.

Given the above assembly, one can fit a set of observations h_j at points $(\mathbf{x}, t)_j, j = 1, 2, \ldots N$, to the spectral functions (4) using the BMK optimal interpolation procedure. From this procedure one obtains smoothed estimates of the signal anomaly at regularly spaced grid points $(\mathbf{x}, t)_i$ given by

$$\hat{h}_i' = \sum_{m=1}^{M} \hat{\lambda}_m f_{mi}, \tag{7}$$

where the $\hat{\lambda}$s are the result of solving M simultaneous linear equations subject to the condition that mean square difference between observations and estimates at the observation points is a

minimum. Formally, the estimated spectral coefficients are comprised of a linear combination of the observations,

$$\hat{\lambda}_n = \sum_{m=1}^{M} \sum_{j=1}^{N} (P+R)^{-1}_{mn} f_{mj}\, \sigma_j^{-2}\, (h-h_0)_j, \tag{8}$$

where we have dropped the double subscript on σ and where

$$R_{mn} = \sum_{j=1}^{N} f_{mj}\, \sigma_j^2 f_{nj}. \tag{9}$$

In general, the estimates $\hat{h}_i$ will differ from the true value h_i by some amount $\delta_i = \hat{h}_i - h_i$, where δ_i is a Gaussian random variable with zero mean and variance

$$E_i^2 = \langle (\hat{h}_i - h_i)^2 \rangle = \sum_{m=1}^{M} \sum_{n=1}^{M} f_{mi}(P+R)^{-1}_{mn} f_{ni}\,. \tag{10}$$

This quantity E_i, sometimes referred to as mapping or interpolation error, depends on the specified signal variance (through P), noise variance (through σ^2), and array geometry (through f_{mj} in R). It does not however depend on the actual values of the observations inasmuch as those observations are consistent with the assumed composition of σ and P.

The conclusions in this paper are based in part on the interpretation of mapped values of E, so it is instructive to consider the behavior of this quantity in two limits. Specifically, consider a situation in which signal and noise are stationary and homogeneous (i.e., $\sigma_j^2 = \sigma^2$ and $P_{mn} = P_{mm}$) and in which the data are uniformly distributed in space and time such that the spectral functions are orthogonal over them (i.e., $\Sigma_j f_{nj} f_{mj} = 0$ if $n \neq m$). Then the mapping error is stationary and homogeneous, and asymptotes to

$$E^2 \sim \begin{cases} \dfrac{M}{N}\sigma^2,\ N \to \infty \text{ or } \dfrac{\langle \lambda_m^2 \rangle}{\sigma^2} \to \infty \text{ for all } m & \text{(11a)} \\[2ex] \displaystyle\sum_{m=1}^{M} \langle \lambda_m^2 \rangle,\ N \to 0 \text{ or } \dfrac{\langle \lambda_m^2 \rangle}{\sigma^2} \to 0 \text{ for all } m. & \text{(11b)} \end{cases}$$

If the number of observations is large or if the signal is strong compared to the noise on the scales of interest, then $E^2 \sim (M/N)\,\sigma^2$; i.e., for a fixed number of spectral functions M, the mapping error variance is proportional to σ^2/N. On the other hand, if the data are sparse or very noisy, $E^2 \sim \Sigma_{m=1}^{M} \langle \lambda_m^2 \rangle$; i.e., the mapping error is limited by the magnitude of variations which have typically occurred in the past. In this latter limit, $\hat{\lambda} \to 0$ and the optimal estimate for h is simply the climatological seasonal mean h_0.

In the following section we present maps of E for the standard and alternate assemblies. In each case we have computed a seasonally averaged E from 1 year (i.e., 4 seasons) of data on the assumption of stationarity in both signal and noise. This allows us to present results for an average season in compact form without the distraction of examining detailed differences, however interesting, from one season to the next.

3. RESULTS

(a) *Simulation of drifting buoy trajectories*

As mentioned earlier, FOCAL will deploy 20 drifting buoys drogued with thermistor chains in the course of a year. The termistor chains will be of sufficient length (115 m) to reach the 20°C isotherm in most of the domain except the far west (Fig. 1). There one could map a slightly shallower isotherm, such as the 23°C isotherm, so that fewer drifter data will be lost for this purpose. For logistical reasons, 4 deployments of 5 buoys each will be made at regular 3-month intervals. How are they best deployed to sample the large-scale low-frequency seasonal variations in the temperature field? The answer to this question is, generally speaking, to deploy them at a location where they will disperse widely to provide good spatial coverage, yet recirculate within the domain to provide long time series. In an attempt to determine the optimal timing and location of these deployments in a rational manner, we have developed a heuristic model of drifting buoy motion which assumes that drifter motions have both a random and deterministic component. The deterministic component is derived from seasonally varying surface currents inferred from historical ship drift data (SCHUMACHER, 1943) whose magnitude we reduced by 20% to account for the effects of wind drag on ships' hulls (STIDD, 1975). Figure 4 shows a summer and winter idealization of these currents projected onto a 2° latitude by 10° longitude grid in which major seasonal fluctuations, such as the summertime appearance of the NECC and intensification of the Guinea Current, are reproduced. Likewise, features such as a slight equatorial surface divergence west of 10°W and a persistent cross-equatorial flow east of 10°W are represented. Continuity in time is established by interpolation between the seasons in Fig. 4 with a smooth 1 cpy cosine curve. We have made no attempt to superimpose on these currents geostrophic perturbations that result from individual realizations of the signal temperature anomaly. Such refinement is unwarranted given that perturbations would be 0 (10 cm s^{-1}), which is comparable to the uncertainty in the ship drift data.

The random component of drifter motion can be physically interpreted as the result of the same noise processes affecting the temperature measurements. It is introduced by integrating

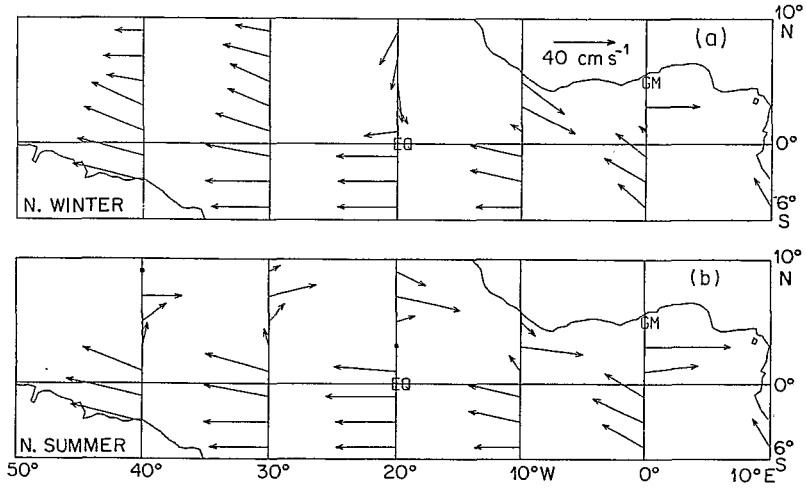

Fig. 4. Mean current vectors derived from historical ship drift data for average conditions in (a) northern winter and (b) northern summer (after SCHUMACHER, 1943).

along a surface trajectory determined by the flow field in Fig. 4 using a second-order Runge–Kutta algorithm with a 10-day time step. After each step the drifter is then displaced randomly in a 50 km "radius of uncertainty" by means of a Guassian random number generator to simulate the dispersive effects of small time and space scales not included in the smoothed Schumacher data. This establishes a new starting point for the next 10-day integration, and the procedure is repeated until the buoy either runs aground, leaves the domain, or expires after an assumed effective lifetime of 1 year. The 10-day time step, together with the 50 km radius of uncertainty, implies an effective lateral diffusivity of about 10^7 cm^2 s^{-1}, the canonical value used in equatorial general circulation models (PHILANDER and PACANOWSKI, 1980, 1981).

Windage on the drifters has been neglected because its effects can not be accurately estimated. We have also neglected the influence of subsurface currents on the thermistor chain. This is reasonable in regimes where there is little current shear below the surface (REVERDIN *et al.*, 1984), but may be less so near the equator, where the current reverses in the upper 100 m. However, the drifter will also have a windowshade drogue at 15 m, so it is likely that most of the drag will be concentrated near the surface in the SEC.

Figure 5 shows four sets of simulated trajectories. In each case deployments took place on 1 January, 1 April, 1 July, and 1 October between 2 and 4°S. Only the longitude of deployment was changed from 5°E to 10°W in 5° increments. The 5°E deployments (Fig. 5a) move quickly across the equator and become entrained in the Guinea Current. Average buoy lifetime before running aground is 155 days, most of which is spent meandering about a convergence zone in the Gulf of Guinea. It is interesting to note that these simulated drifters behave in much the same way as real drifters deployed by PITON and FUSEY (1982) at 5°W, 2°S, which became rapidly entrained in the Guinea Current, then meandered for several months in the eastern Gulf of Guinea. The 0°W deployments spread further west, although the northernmost drifters entering the water are again quickly entrained into the Guinea Current (Fig. 5b). By contrast, the 5°W deployments (Fig. 5c) spread more uniformly to the east and west than either the 5°E, 0°W, or 10°W (Fig. 5d) deployments, with drifters from the latter seldom recirculating to the east of 30°W via the NECC. The average drifter lifetime for the 5°W deployments is 244 days, longer by about 2 months than the 10°W deployments, and longer by about 3 months than the 5°E deployments. The fact that the 5 and 0°W lifetimes are comparable is misleading, because the latter is inflated by several drifters that spend almost a year each meandering in the Gulf of Guinea without running aground. One can also see in Fig. 5c the seasonality of the NECC. Drifters launched in January and April reach the central basin in summertime when the NECC is strongest, and they are subsequently swept eastward. By contrast, those arriving in winter from the July and October deployments are advected westward in the absence of the NECC and eventually leave the domain.

Different realizations of the random flow component result in trajectories similar to those shown in Fig. 5, with average drifter lifetimes agreeing to within 1 month. Suppressing the random component altogether smooths out individual trajectories, but does not significantly alter the shape of the trajectory envelopes. Likewise, if one assumes that drifters move 25% slower due to deep drag on the thermistor chains, lifetimes increase correspondingly, but there are no especially remarkable changes in dispersal patterns. Based on these experiments, we therefore conclude that 5°W deployments of FOCAL drifters will provide the best spatial and temporal coverage of thermocline depth variations.

We performed a number of simulations to investigate the importance of timing and

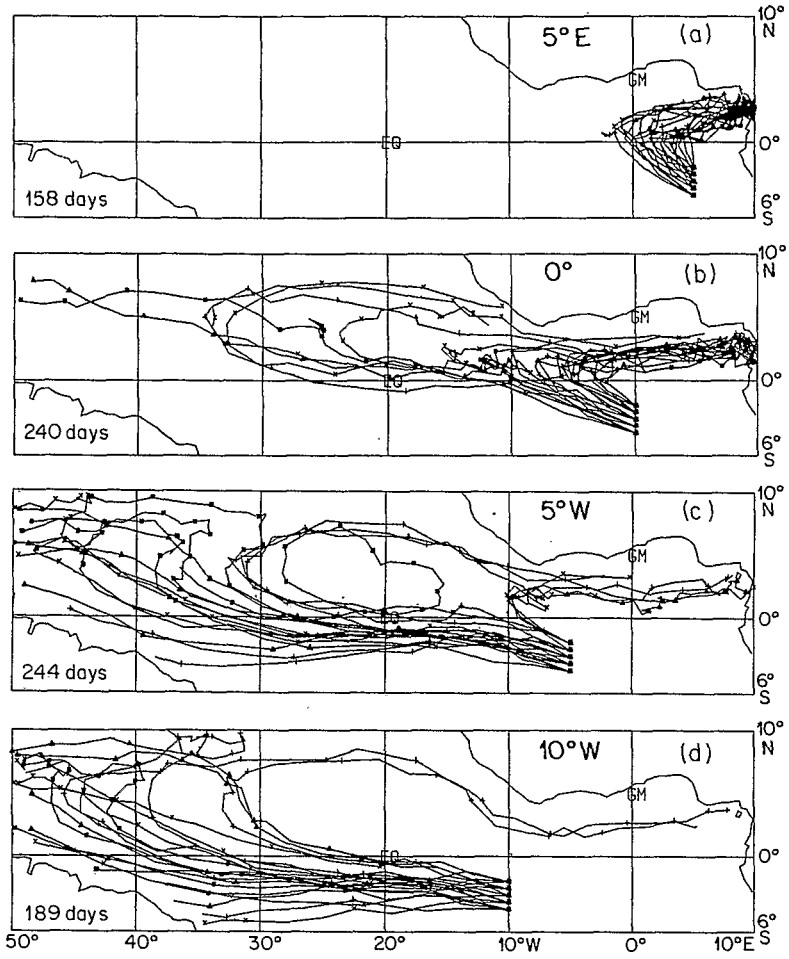

Fig. 5. FOCAL drifting buoy trajectories for deployments made between 2 and 4°S on 1 January (×), 1 April (+), 1 July (■), and 1 October (▲) from (a) 5°E, (b) 0°W, (c) 5°W, and (d) 10°W. Symbols are spaced at 30-day intervals along trajectories. Average drifter lifetime in days is indicated at lower left.

latitudinal spacing on deployments at 5°W. Changing the launch time but maintaining a 3-month interval between successive launches had less of an effect than changing the longitude of deployment. Spreading the drifters between 0 and 4°S on deployment reduced dispersal because the northernmost buoys quickly moved into the Gulf of Guinea. Spreading the buoys between 2 and 6°S on deployment shifted the data coverage to the south, but did not significantly affect average lifetimes. Thus we conclude that timing of deployments is less critical than choosing the correct longitude, but that deployments should be made south of the equator to avoid rapid entrainment in the Guinea Current.

We repeated a number of the above simulations with monthly ship drift data from the SCHUMACHER (1943) atlas instead of the more highly smoothed version in time shown in Fig. 4. The major differences are that when using monthly current data, a few more drifters

deployed at 0°W and the southernmost drifters deployed at 5°E in spring escape to the western basin. Overall, however, the basic dispersal patterns are similar, and our conclusions with respect to deployment strategy do not change.

(b) *Expected errors for the standard assembly*

Figure 6 shows maps of expected error in 20°C isotherm depth on seasonal time scales for four different array configurations and Table 2 summarizes the performance of these arrays. Also listed in Table 2 is the number of independent observations each platform contributes on average per 3-month season. Unless otherwise specified, all results are for a frequency cutoff at $\omega = 1$.

Figure 6a shows that for the array composed of XBTs and tide gauges (which we will designate as a monitoring array), expected error is lowest in the vicinity of the platforms, increasing rapidly into data void regions. The 5-m contour encloses only 5% of the domain in

Table 2. Performance of different arrays in terms of percentage of the equatorial Atlantic with expected random mapping error <3 and 5 m. Also shown are the number of independent samples each platform contributes on average per 3-month season

Array		Average No. of independent data per 3-month season	% of domain with $E \leqslant$ 3 m	% of domain with $E \leqslant$ 5 m
1. Monitoring				
(a) XBT		47		
(b) Tide gauge		33		
	Total	80	0 (0)*	5 (4)*
2. FOCAL/SEQUAL				
(a) XBT		47		
(b) Tide gauge		20		
(c) CTD		65		
(d) IES		47		
(e) Mooring		42		
	Total	221	3	65
3. FOCAL/SEQUAL Drifter augmented				
(a) XBT		47		
(b) Tide gauge		20		
(c) CTD		65		
(d) IES		47		
(e) Mooring		42		
(f) FOCAL drifter		91		
	Total	312	16 (6)†	89 (78)†
4. FOCAL/SEQUAL Drifter augmented, mooring depleted				
(a) XBT		47		
(b) Tide gauge		27		
(c) CTD		65		
(d) IES		47		
(e) FOCAL drifter		91		
	Total	277	1	89

* The standard assembly modified to include a 2 cpy component.
† An alternate assembly with inhomogeneous signal and noise statistics. See text for discussion.

an area where XBT tracks cross and where two tide gauges are located. The patterns and magnitudes in this figure change little if, keeping the total signal variance fixed at $(15\ \mathrm{m})^2$, we include a 2 cpy frequency component with 1/4 of the 1 cpy variance. This is evident in Table 2, where one sees very little change in the total area enclosed by the 5-m contour. Based on this comparison we hereafter restrict our discussion exclusively to the $\omega = 1$ frequency cutoff because, for a red spectrum, explicit inclusion of higher harmonics will not significantly alter our seasonal estimates.

One can contrast the accuracy of the monitoring array with that of the FOCAL/SEQUAL array during the 2-year intensive sampling period (Fig. 6b). Expected errors are reduced to as little as 3 m r.m.s. in restricted regions along the equator, which is now heavily sampled by moorings, IES, and repeated CTD sections. Correspondingly, the 5-m contour encloses 65% of the domain. Note that 13 fewer tide gauge data per season are included in this array compared to the monitoring array. This is primarily due to the fact that a mooring is in close proximity to the tide gauge at St. Peter and Paul rocks (1°N, 29°W), so that the latter has been discarded as redundant instrumentation in the analysis. Figure 6c shows the expected error for the FOCAL/SEQUAL array augmented by drifter data from the 5°W deployment in Fig. 5c. The 3-m and 5-m contours now enclose 16 and 89% of the domain, respectively (Table 2). This is a significant improvement over the array without FOCAL drifters, and is due to the fact that drifting buoy data now account for 30% of all data and make the largest single contribution to the total. Moreover, one can extract the 6 moorings, which in total cost 5 times more than the drifters, with little noticeable loss in accuracy (Table 2; Fig. 6d). The only difference is that for the mooring depleted array the 3-m contour evident in Fig. 6c essentially disappears in the immediate vicinity of the equator. Thus, one can argue that drifters are a more effective means of determining large-scale seasonal fluctuations than moored instrumentation. This of course is not meant to devalue the usefulness of moorings. Eulerian time series are indispensable for providing finely resolved frequency spectra of both temperature and velocity at fixed locations, and they are easier to interpret than Lagrangian data. Our results simply state the obvious in a quantitative manner, namely that Lagrangian measurements provide better spatial coverage than would be possible from a fixed array.

(c) *Expected errors for an alternate assembly*

The validity of our *a priori* error estimates can be questioned because the assumed standard assembly statistics are not unambiguously defined from historical data analyses. One could plausibly argue for alternative assemblies in which, for example, noise levels are higher near the equator than either north or south due to the presence of an energetic equatorial wave continuum at periods between 1 day and 1 month (ERIKSEN, 1980) and/or due to the presence of equatorial basin modes (GENT, 1979). Likewise, by analogy with mid-latitudes, one could argue for more mesoscale variability to the west than to the east (DANTZLER, 1977). With regard to signal variability, it is conceivable that seasonal anomalies are larger in the vicinity of the NECC and west of 20°W along the equator given that the annual cycle is most intense in these regions (MERLE, 1980; KATZ, 1981).

We have incorporated these viewpoints into an alternate assembly in which (1) noise levels are 15 m on a basin-wide average, but 18.75 m between 2°N and 2°S, 18.75 m west of 30°W, and 11.25 m elsewhere; and (2) signal amplitude increases linearly by a factor of 2 from 15 m r.m.s. in the extreme southeast to 30 m r.m.s. in the extreme northwest. Figure 7a shows the expected error based on this assembly for the drifter-augmented FOCAL/SEQUAL array. The total area enclosed within the 3- and 5-m contours is now smaller,

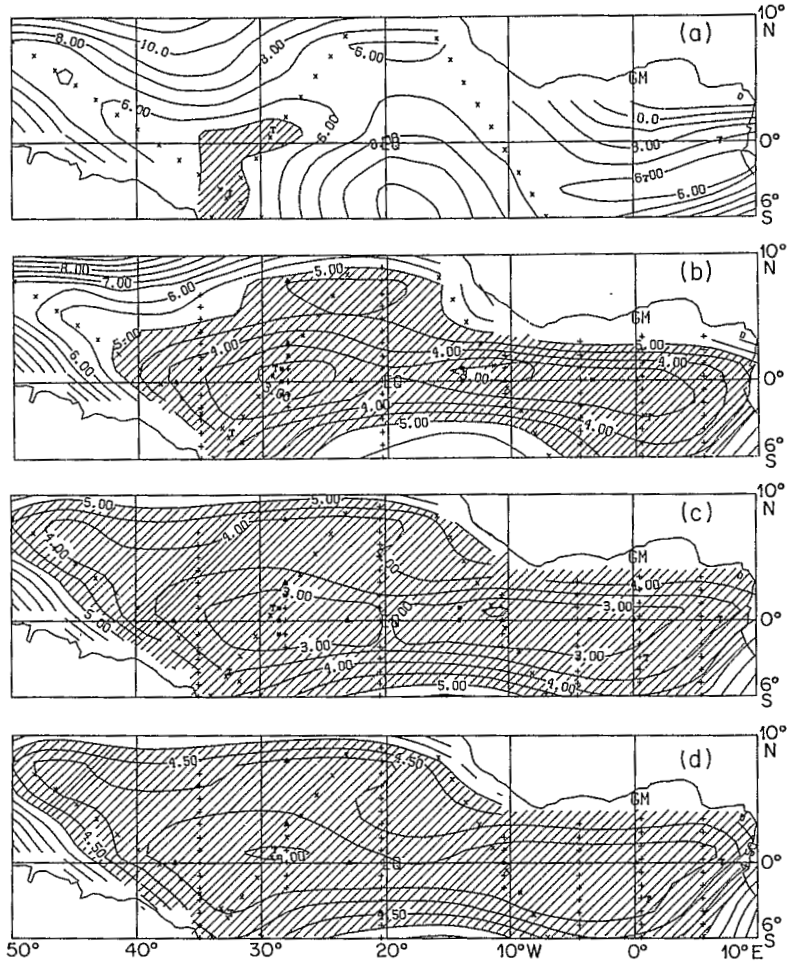

Fig. 6. Expected random error, E, in maps of 20°C isotherm depth on seasonal time scales for (a) the long-term array, (b) FOCAL/ SEQUAL array without FOCAL drifters. (c) FOCAL/SEQUAL array augmented by FOCAL drifters deployed as in Fig. 5c at 5°W, 2 to 4°S, and (d) FOCAL/ SEQUAL array augmented by FOCAL drifters but depleted of moorings. Platforms are indicated by (X) for XBT, (T) for tide gauge, (+) for CTD, (▲) for inverted echo sounders, and (■) for moorings. Sample rates are shown in Table 1 along with the weight given to each type of measurement. Table 2 lists data counts. Contour interval is 1 m for (a) and 0.5 m for (b) to (d).

though the 5-m contour still encloses more than 3/4 of the domain. Compared to the standard assembly, expected errors have increased by 0 (1 m) along the equator and west of 30°W, and decreased by a corresponding amount elsewhere (Fig. 7b). These differences can be rationalized in terms of (11), namely that in general the domain is sufficiently well sampled that E varies linearly with σ. However, there are regional deviations from a strict linear dependence which are correlated with data density. In particular, based on a series of experiments in which signal and noise levels were systematically changed one at a time, it was found that where $N \gtrsim 10$ observations per season per 2° latitude by 10° longitude box (e.g., along

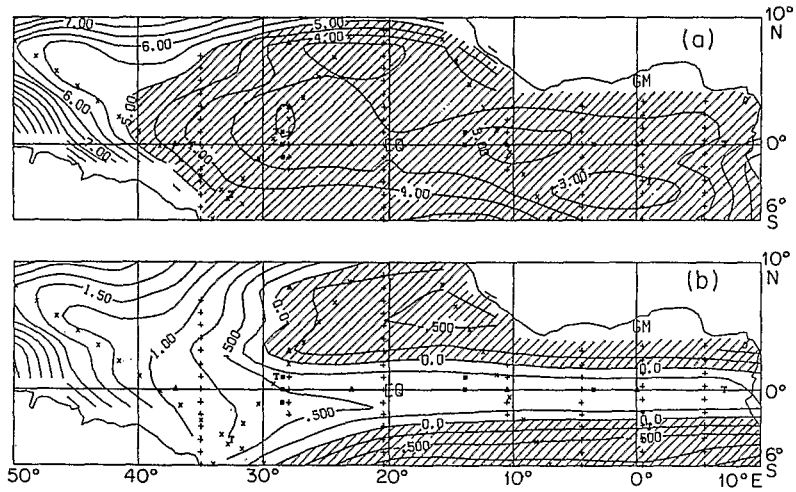

Fig. 7. (a) Same as in Fig. 4c except for assembly statistics discussed in Section 3b, and (b) differences between this map and that in Fig. 4c. Shading indicates areas where errors based on the alternate assembly are smaller than those based on the standard assembly. Contour interval is 0.25 m in (b).

the equator), E usually varied linearly with σ to within 10%. Conversely, where $N \ll 10$ observations (e.g., in areas of the northwest and southwest), E varied more slowly with σ and was sensitive to changes in P, indicating the influence of assumed signal levels on error estimates.

4. SUMMARY AND DISCUSSION

In the foregoing sections we formulated an objective analysis procedure based on optimal interpolation for mapping the depth of the 20°C isotherm on seasonal time scales. We then used this procedure to specifically address the question of expected accuracy in such maps based on an array of XBTs, CTDs, tide gauges, IES, mooring and drifting thermistor chains. We also sought to determine the best location and time to deploy 20 FOCAL drifting buoys as temperature sensors drogued with termistor chains. Consideration of this latter issue required the development of a heuristic model of drifting buoy motion based on random and deterministic components of the surface flow field.

Our results indicate that the FOCAL/SEQUAL temperature sensor array will achieve an accuracy of 5 m over a large percentage of the region 10°E to 50°W, 6°S to 10°N during the 2-year intensive sampling period of 1982 to 1984. Moreover, FOCAL drifters contribute significantly to this accuracy when deployed at 5°W between 2 and 4°S in four installments of five each at 3-month intervals. Timing of the initial deployment does not appear to be critical. However, the longitude of deployment significantly affects the ultimate dispersal pattern of the drifters, with deployments further to the east or to the west providing less uniform space/time coverage in the equatorial zone. That these drifters are cost-effective measurement platforms is evident from the fact that a total of about 30 independent estimates per year of the seasonal cycle from a $10,000 drifter translates into about $300/datum (excluding shiptime), whereas the same number of estimates from a $100,000 mooring costs about

$3000/datum. This neglects the other valuable uses of mooring data, but it does illustrate the value of drifting buoys for observing large-scale, low-frequency oceanic phenomena. Of course, XBTs are the least expensive array element (about $50/datum), but a measurement program based solely on three shiptracks repeated every 2 months and 4 tide gauges, while suitable for long-term monitoring purposes, would not provide an adequate data base for critically testing dynamical hypotheses concerning the equatorial response to seasonal wind forcing.

Our conclusions with respect to estimated random mapping errors are for the most part based on a standard assembly, i.e., an assumed set of statistics describing the spectrum of variability in the equatorial Atlantic. However, not all aspects of this assembly are well defined from historical data analysis. We therefore considered a plausible alternative to this standard and found 0 (1 m) differences in error estimates for the FOCAL/SEQUAL array augmented with FOCAL drifters. These estimates were furthermore found to be more sensitive to assumed observational noise levels rather than signal levels, suggesting an asymptotic behavior for E similar to (11a) for data coverage of $\gtrsim 10$ observations per season per 2° latitude by 10° longitude box.

Bias errors, which we have not explicitly considered in this study, can arise from three sources (BMK): (1) poorly calibrated instruments; (2) poorly known seasonal climatology in regions where the array provides little new information; and (3) misrepresentation of the assembly statistics used in the objective analyses. We can discount the first of these, because careful intercalibration studies will be done as part of FOCAL/SEQUAL. On the scales we have considered in this study, the second of these should be small for the intensive sampling period, because estimates of the signal field will be weighted more by new information than by climatological data over large areas of the domain based on sample density. For a very sparse array like the monitoring array, however, biases of this type could be more severe. The third source of bias should likewise be small, even though neither signal nor noise statistics are unambiguously defined from previous data analyses. This is because assembly statistics can be updated *a posteriori* after the field experiment has terminated by means of a Bayesian approach outlined in BMK. The procedure is essentially a sophisticated extension of the more conventional approach used in least squares analysis for hypothesis testing in which squared residuals about different regression models are compared using an F-test. In this way one is able to distinguish which of several possible assemblies is most consistent with the observations themselves and which therefore should be used in mapping.

The exact spectral cutoff in (4) is dictated by computational limitations. We have chosen to do a combined frequency-wavenumber analysis for which 135 spectral functions are required if the frequency cutoff is at 2 cpy, or 81 are required if the cutoff is at 1 cpy. The advantage of this approach is that it allows fluctuations to be represented smoothly and continuously in both space and time. The disadvantage is that this description of space/time variability is effectively restricted to the lowest order spectral components because of computational efficiencies involved in solving for all spectral amplitudes (λ) simultaneously. This is not a severe limitation if indeed the spectrum is red, as we demonstrated in comparative analyses with and without energy at 2 cpy. On the other hand, to draw more finely resolved maps in space and time—maps, for example, with a resolution of 1° latitude, 5° longitude, and 1 month—it may be more advantageous to abandon the combined frequency-wavenumber approach and treat each month individually. This would allow explicit treatment of the higher wavenumbers at significant computational savings. Such maps would certainly be less accurate than more coarsely resolved seasonal maps because there would effectively be fewer

data available for defining a broader spectral band of spatial variability. Nonetheless, higher resolution maps may be more desirable for some applications.

Acknowledgements—The authors gratefully acknowledge the financial support for this study provided by the Centre National de la Recherche Scientifique, the Centre National d'Exploration des Oceans, and the Joint Institute for the Study of the Atmosphere and Ocean. We are indebted to Joseph Gonella of the Laboratoire d'Oceanographie Physique, Museum National d'Histoire Naturelle in Paris, who as principal investigator of the FOCAL drifting buoy program, originally suggested this work. We are also thankful to those individuals who provided valuable insights throughout the course of this work, especially Francois Jarrige of the Antenne ORSTOM, Centre Oceanologique de Bretagne, and Joel Picaut of the Universite de Bretagne Occidentale in Brest, France. We likewise acknowledge Francis Bretherton of the National Center for Atmospheric Research, and Eric Kraus of the Cooperative Institute for Research in the Environmental Sciences, both of Boulder, Colorado, who were instrumental in initiating this work. JISAO Contribution No. 12.

REFERENCES

ANONYMOUS (1982) SEQUAL: a study of the equatorial Atlantic Ocean. In: *EOS, Transactions of the American Geophysical Union*, **64**, No. 14.

BESSIS J. L. (1982) Le Systeme ARGOS. In: *Proceedings of ARGOS Users Conference*, Paris, 20–22 April 1982, WMO-CNES, pp. 1–10.

BRETHERTON F. P., R. E. DAVIS and C. B. FANDRY (1976) A technique for objective analysis and design of oceanographic experiments applied to MODE-73. *Deep-Sea Research*, **23**, 559–582.

BRETHERTON F. P., M. J. McPHADEN and E. B. KRAUS (1984) Design studies for climatological measurements of heat storage. *Journal of Physical Oceanography*, **14**, in press.

CANE M. A. and E. S. SARACHIK (1981) The response of a linear baroclinic equatorial ocean to periodic forcing. *Journal of Marine Research*, **39**, 651–693.

CRESSMAN G. P. (1959) An operational objective analysis system. *Monthly Weather Review*, **87**, 367–374.

DANTZLER H. L., JR. (1977) Potential energy maxima in the tropical and subtropical Atlantic. *Journal of Physical Oceanography*, **7**, 512–519.

DRAPER N. R. and H. SMITH (1966) *Applied regression analysis*, John Wiley, New York, 407 pp.

DÜING W., P. HISARD, E. KATZ, J. KRAUSS, J. MEINCKE, L. MILLER, K. MOROSHKIN, G. PHILANDER, A. RYBNIKOV, K. VOIGHT and R. WEISBERG (1975) Meanders and long waves in the equatorial Atlantic. *Nature, London*, **257**, 280–284.

ERIKSEN C. C. (1980) Evidence for a spectrum of equatorial waves in the Indian Ocean. *Journal of Geophysical Research*, **85**, 3285–3303.

GANDIN L. S. (1965) *Objective analysis of meteorological fields*, translated from the Russian by the Israeli Program for Scientific Translations, 242 pp.

GENT P. (1979) Standing equatorial wave modes in bounded ocean basins. *Journal of Physical Oceanography*, **9**, 653–662.

KATZ E. J. (1981) Dynamic topography of the sea surface in the equatorial Atlantic. *Journal of Marine Research*, **39**, 63–63.

KATZ E. J., R. BELEVITSCH, J. BRUCE, V. BUBNOV, J. COCHRANE, W. DÜING, P. HISARD, H. U. LASS, J. MEINCKE, A. DEMESQUITA, L. MILLER and A. RYBNIKOV (1977) Zonal pressure gradient along the equatorial Atlantic. *Journal of Marine Research*, **35**, 293–307.

KATZ E. J., R. L. MOLINARI, D. E. CARTWRIGHT, P. HISARD, H. U. LASS and A. DEMESQUITA (1981) The seasonal transport of the Equatorial Undercurrent in the Western Atlantic (during the Global Weather Experiment). *Oceanologica Acta*, **4**, 445–450.

LORENC A. C. (1981) A global three-dimensional multivariate statistical interpolation scheme. *Monthly Weather Review*, **109**, 701–721.

MCCREARY J. P., JR., J. PICAUT and D. W. MOORE (1984) Effects of remote annual forcing in the eastern tropical Atlantic Ocean. *Journal of Marine Research*, **42**, 45–81.

MERLE J. (1980) Seasonal heat budget in the equatorial Atlantic. *Journal of Physical Oceanography*, **10**, 464–469.

MERLE J. (1983) Seasonal variability of subsurface thermal structure in the tropical Atlantic Ocean. In: *Proceedings of the 14th Annual Liege Colloquium on Ocean Hydrodynamics*. J. C. G. NIHOUL, editor, Elsevier, Amsterdam, pp. 31–50.

MILLER L. (1981) Acoustic measurements of dynamic height and wind speed in the eastern equatorial Atlantic. In: *Recent progress in equatorial oceanography: a Report of the Final Meeting of SCOR Working Group 47*, Nova University, pp. 325–334.

MOORE D. W., P. HISARD, J. P. MCCREARY, J. MERLE, J. J. O'BRIEN, J. PICAUT, J. M. VERSTRAETE and C. WUNSCH (1978) Equatorial adjustment in the eastern Atlantic. *Geophysical Research Letters*, **5**, 637–640.

PHILANDER S. G. H. (1979) Upwelling in the Gulf of Guinea. *Journal of Marine Research*, **37**, 23–33.
PHILANDER S. G. H. and R. C. PACANOWSKI (1980) The generation of equatorial currents. *Journal of Geophysical Research*, **85**, 1123–1136.
PHILANDER S. G. H. and R. C. PACANOWSKI (1981) Response of equatorial oceans to periodic forcing. *Journal of Geophysical Research*, **86**, 1903–1916.
PITON B. and F.-X. FUSEY (1982) Trajectories of two satellite tracked buoys in the Gulf of Guinea, July 1978–July 1979. *Tropical Ocean–Atmosphere Newsletter*, No. 10, University of Washington.
REVERDIN G., J. GONELLA and J. F. MURAIL (1984) Etude comparative de derive de buoees avec et sans chain de thermistances, submitted to *Oceanologica Acta*.
SCHUMACHER A. (1943) Monatskarten der Oberflachenstromungen im aquatorialen und sudlichen Atlantischen Ozean. *Annalen der Hydrographie u. Maritime Meteorologie*, **71**, 209–219.
SEAVER G. A. and S. KULESHOV (1982) Experimental and analytical error of the expendable bathythermograph. *Journal of Physical Oceanography*, **12**, 592–600.
STIDD C. K. (1975) Meridional profiles of ship drift components. *Journal of Geophysical Research*, **80**, 1679–1682.
WEISBERG R. (1979) Equatorial waves during GATE and their relation to the mean zonal circulation. *Deep-Sea Research*, **26**, GATE Suppl. II, 179–198.
WHITE W. B., G. MEYERS and K. HASUNUMA (1982) Space/time statistics of short term, climatic variability in the western North Pacific. *Journal of Geophysical Research*, **87**, 1979–1989.
WYRTKI K. (1974) Sea level and seasonal fluctuations of the equatorial currents in the western Pacific Ocean. *Journal of Physical Oceanography*, **4**, 91–103.